

Article

# CFD Validation of a Model Wind Turbine by Means of Improved and Delayed Detached Eddy Simulation in OpenFOAM

Camilo A. Sedano <sup>1,2,\*</sup>, Frederik Berger <sup>3</sup>, Hamid Rahimi <sup>1,3</sup> , Omar D. Lopez Mejia <sup>2</sup>   
and Martin Kühn <sup>3</sup> and Bernhard Stoevesandt <sup>1</sup> 

<sup>1</sup> Fraunhofer IWES, Küpkersweg 70, 26129 Oldenburg, Germany; hamid.rahimi@uni-oldenburg.de (H.R.); bernhard.stoevesandt@iwes.fraunhofer.de (B.S.)

<sup>2</sup> Department of Mechanical Engineering, Universidad de los Andes, Cra 1 Este N 19A-40, Bogotá 111711, Colombia; od.lopez20@uniandes.edu.co

<sup>3</sup> Institute of Physics, ForWind—University of Oldenburg, Küpkersweg 70, 26129 Oldenburg, Germany; frederik.berger@uni-oldenburg.de (F.B.); martin.kuehn@uni-oldenburg.de (M.K.)

\* Correspondence: ca.sedano1167@uniandes.edu.co; Tel.: +57-315-3927-393

Received: 24 January 2019; Accepted: 5 March 2019; Published: 4 April 2019



**Abstract:** With the ongoing increase in the size of wind turbines, experimental investigations have become more complicated and expensive. Therefore, computational models have proven to be a viable solution for design purposes. This article aims to validate CFD simulations of an experimental model wind turbine (MoWiTO 1.8) using Delayed Detached Eddy Simulation (DDES) and Improved DDES (IDDES) turbulence modelling approaches. For the purpose of validation, integral quantities (such as power, thrust, torque and blade-root bending moment in the flapwise direction) measured in the wind tunnel are compared with numerical results obtained with OpenFOAM. In general, the computational results show a very good agreement with the measurements for most of the monitored quantities. In particular, the blade-root bending moment presents the largest difference, taking into account that the simulation assumes the turbine blades are rigid. Nevertheless, the simulation does achieve in recreating the turbulent behavior as can be evidenced by the Power Spectral Density graphs, and the wake's velocity measurements. In general, the IDDES turbulent model achieves a better agreement to the experimental results, while maintaining a very similar computational time as the DDES model.

**Keywords:** computational fluid dynamics; OpenFOAM; DDES; MoWiTO 1.8; wind turbine aerodynamics

## 1. Introduction

With larger wind turbines it is possible to reduce the levelized cost of energy (LCoE). This is why one of the main trends in wind energy has been to further increase the size of turbines. However, this in turn implies several complications. First of all, by increasing the rotor's diameter, wind turbine loads start to have a larger influence on their structural design, thus on their cost [1]. In research projects such as the AVATAR project [2], turbines of 10 MW or larger are being studied. With turbines of such sizes it then becomes complicated and expensive to do experimental analysis. There have been two main approaches to solving this issue: scaled model turbines with which experimental analysis can be performed in wind tunnels under controlled conditions and through numerical methods.

While on the one hand, the experimental model turbines can reproduce to some extent the actual phenomena that are taking place, this is highly dependent on a correct scaling process. On the other hand, numerical methods attempt to solve the equations governing the physics of these phenomena. However, to do so, they usually use different models and simplifications in order to reduce the computational cost. It is clear then that even though both approaches are able to obtain results

which are comparable to the physical phenomena taking place, they are not 100% accurate. Therefore, by doing a joint effort of calibrating the computational models by comparing them to experimental results from scaled turbines, relevant analysis and conclusions can be obtained. The importance of validating the computational models relies on the increasing interest in these tools and studies such as the ones performed by Rahimi et al. [3,4]. In these investigations, the authors are constantly evaluating the simulations performed, by doing comparisons with experimental measurements in order to validate the numerical results.

One of the most renowned turbine models is the NREL Phase VI turbine [5]. Various authors have used this model turbine as a benchmark case study with which to compare computational results. Such is the case of Sorensen et al. who in 2002 performed a computational analysis to evaluate the results obtained using the EllipSys3D software [6]. In addition, in 2014 the same authors used a DDES turbulent model [7], achieving comparable results in both cases. In a similar way, Zahle et al. [8] performed a computational model of this turbine with the same software. In this study, the authors used an overset grid method for the computational mesh with good success. The main purpose with this meshing method was to include the interaction between rotor and tower, achieving good agreement when comparing the experimental results to the computational ones [8]. More recently, Rahimi et al. performed a computational study on the use of the free licensed software OpenFOAM for this type of application, focusing on the importance of the mesh quality [9]. Langer-Moller et al. used the THETA code to reproduce some of the experimental results obtained from the NREL Phase VI turbine comparing a compressible and an incompressible implementation [10].

Most of these works have usually used Reynolds Average Navier-Stokes (RANS) or DES turbulence model as is the case for [6,8,10]. These type of RANS turbulent models usually have a relatively low computational cost, however, they do present different problems. Particularly, RANS models are not as accurate as in the separated flow, while the DES models are unable to resolve the turbulence near the boundary layer [11]. Nowadays, with the ongoing increase in computational capacity, it is possible to use hybrid models such as DDES and IDDES. However, these models have been just recently studied in wind turbine aerodynamics, for example, in studies by Sorensen et al. [7] or Rahimi et al. [12]. Therefore, it is necessary to further investigate how accurate these turbulent modelling techniques can be.

Recently at ForWind—University of Oldenburg, a new model turbine was developed, scaled from the NREL 5 MW turbine [13]. The 1.8 diameter Model Wind Turbine Oldenburg (MoWiTO 1.8), mimics similar aerodynamic characteristics to the NREL 5 MW turbine. It has pitch and torque controllers, while being able to measure the power, torque and thrust from the turbine, as well as blade root bending moments [13]. Experiments were performed in the wind tunnel at the University of Oldenburg. The data obtained in these experiments was used for comparison with the numerical simulation presented here. The principal aim of this work is then to validate the numerical results obtained with OpenFOAM with the experimental results from the wind tunnel. Furthermore, this work also attempts to compare the results from using a DDES and an IDDES turbulent model respectively. Knowing that both models are intended to study massive flow separation phenomena, this study attempts to study a safe operation condition (i.e., no yaw and small blade pitch angle). This way, it could work as a reference point to compare against, when studying more critical conditions at which the turbine could stall.

## 2. Methods

### 2.1. Experimental Setup

For the current study, CFD simulations are compared to wind tunnel measurements, with an experimental model wind turbine, of the global turbine parameters: power, torque, thrust and flap-wise blade root bending moments, as well as the flow in the near wake. The recently developed

Model Wind Turbine Oldenburg with 1.8 m diameter (MoWiTO 1.8) (see also [13]) is used in the large wind tunnel of the University of Oldenburg for comparison or validation.

The aerodynamic design of the rotor blades is based on a scaling approach of the NREL 5 MW turbine [14]. With this approach, the design tip speed ratio of the rotor is kept, as well as the ratio of lift distribution along the radius, as is described in detail in Berger et al. [13]. The rotor radius was scaled down by a factor of 70, thus also the chord based Reynolds number is decreased similarly. To account for this lower Reynolds number, the scaled rotor blade is based on the low Reynolds number airfoil profiles SG6041 and SG6041 [15]. These profiles operate well at the decreased chord based Reynolds number, which ranges from  $60 \times 10^3$  at the blade root to  $120 \times 10^3$  at the blade tip, for the experimental parameters used in the present study.

The nacelle of the turbine is shown in Figure 1a and the turbine with a size reference in Figure 1b. The rotor blades are made from carbon fiber with individual pitch motors at the blade root. The flap-wise blade root bending moments are obtained by full Wheatstone bridge strain gauges. Signals are transferred by a slip ring from the rotating to the stationary nacelle system. The rotational speed and azimuthal position are obtained by encoders. The rotor torque is measured by a torque sensor and the tower foot bending moment in fore-aft direction is recorded by strain gauges. These moments are corrected for the tower and nacelle drag by measurements without rotor blades. From these corrected moments, the rotor thrust is derived. In addition, the torque is corrected for drivetrain losses in the bearings and the slip ring. The control and data acquisition is handled with a CompactRIO PAC system and programmed in LabVIEW.

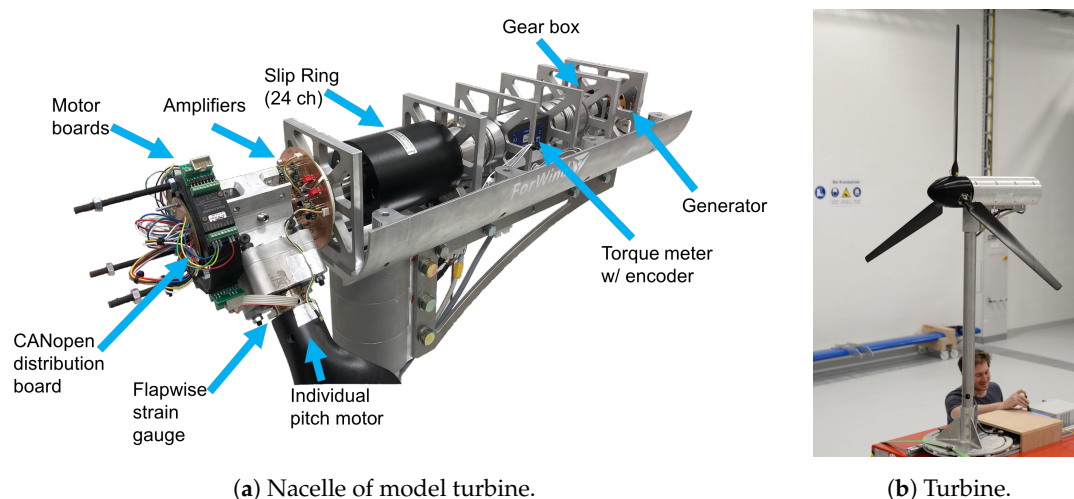
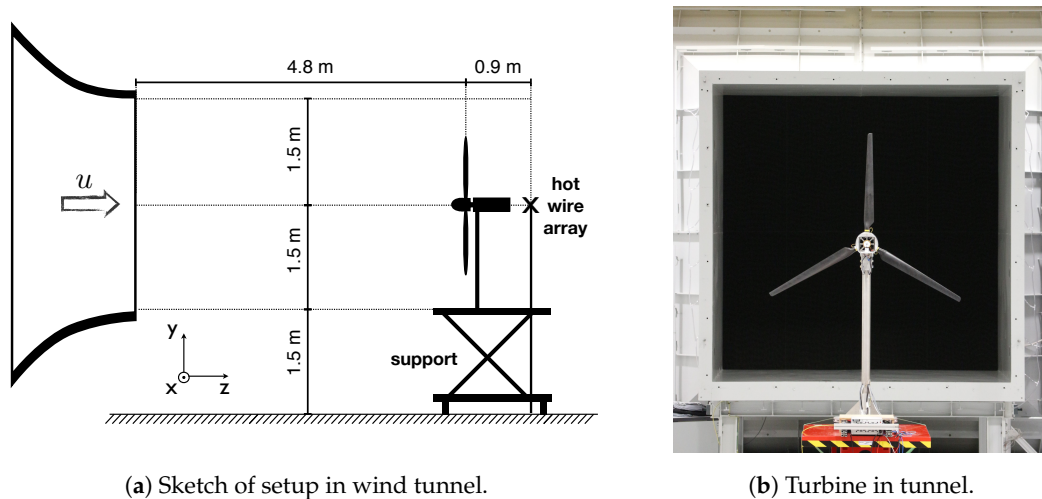


Figure 1. MoWiTO 1.8.

The model wind turbine is placed in the Göttingen type wind tunnel in the WindLab building of the University of Oldenburg, with an open jet configuration, as sketched in Figure 2a. The nozzle of the tunnel has an outlet of 3 m by 3 m and a test section length of 30 m. Wind speeds of more than 32 m/s can be achieved in the wind tunnel test section, in the open jet configuration.

The rotor plane is located 4.8 m, i.e., 2.7 rotor diameter ( $D$ ), behind the tunnel outlet. The nacelle is placed centered in the  $x$ - $y$  plane (see coordinate system in Figure 2a) to the tunnel outlet as shown in Figure 2b. In the near wake, at a distance of 0.9 m behind the rotor plane (i.e., 0.5  $D$ ) hot wire measurements have been performed at hub height at eight different lateral positions from 0  $R$  to 1.4  $R$  in steps of 0.2  $R$ . The signals of hot wires, strain gauges at blade root and tower bottom as well as rotor torque are recorded synchronously at a sampling frequency of 5 kHz.

For the comparison within this study, one stationary operational point with a pitch angle of  $1^\circ$  at 6.03 m/s and 480 rpm has been considered, corresponding to design conditions at a tip speed ratio of 7.5.



**Figure 2.** Turbine setup in tunnel.

## 2.2. Computational Methods

The OpenFOAM 4.0 software was used [16]; in particular the ‘pimpleDyMFoam’ solver. This solver uses the PIMPLE algorithm to iterate the solution of the pressure and velocity coupling [17]. In this case, since it is a blade resolved simulation, it was necessary to use a dynamic mesh (DyM) in order to account for the rotation of the blades, assuming this has a constant speed. A passive dynamic mesh model is used, in such a way that the rotation of the blades is constant and independent of the flow’s effects. All simulations were run in the High Power Cluster (HPC) EDDY at the University of Oldenburg [18].

### 2.2.1. Simulation Settings

Two sets of blade resolved type simulations (DDES and IDDES) were performed. In both sets of simulations, the PIMPLE algorithm was solved using a Gauss upwind scheme, with a second order backward time discretization. The first set is intended to study the time convergence of the simulation. To do so, three different simulations were made with different time steps:  $0.1^\circ$  of azimuthal rotation per time step,  $0.5^\circ$  of rotation per time step and  $1^\circ$  of rotation per time step ( $3.47 \times 10^{-4}$  s,  $1.74 \times 10^{-4}$  s and  $3.47 \times 10^{-5}$  s, respectively). This way it could be evaluated which setup would yield agreeable results without incurring higher computational costs. This set of simulations was performed using a DDES turbulent model.

Once the time convergence analysis was performed, a new simulation was done in order to compare the results obtained between a DDES and an IDDES turbulence model. The purpose was to confirm which of the two turbulent approaches would yield the closer results in comparison to the experimental measurements.

All simulations were performed assuming the blades are rigid. Based on the design FEM calculations of the rotor blades, we estimated that the tip deflection for the considered operational point would be in the order of 8 mm. Therefore, the tip deflection is less than 1% of the blade radius. In comparison, the NREL 5 MW turbine has a tip deflection of 6% near rated operation [14]. The normalised tip deflection of the model turbine is thus much lower than for the reference turbine and we expect no relevant influence of the model turbine blade tip deflection on the aerodynamic behaviour and thus considered the blade in these simulations to be perfectly stiff.

### 2.2.2. Improved and Delayed Detached Eddy Simulation

The DDES approach couples the advantages of the LES turbulent approach in the far field region, with the RANS approach in the attached boundary layer regions. This was done taking into account that the LES approach has had some complications solving the flow characteristics near the boundary

layer [11]. At first, the DES mainly showed advantages by being a model that is not zonal, while using a one-equation model to solve for the turbulence (i.e., the Spalart-Allmaras model) [19]. However, this first implementation was highly dependent on grid spacing. In order to counteract for the artificial reduction of eddy viscosity, Spalart then proposed the DDES by using a blending function to define the length scale. In this case, the eddy viscosity value would work as the detection mechanism to shift from RANS to LES [20]. Therefore, the DDES approach looks to transition from a RANS model (in this case the  $k - \omega$  SST model was used) near the boundary layer of the turbine, to a LES model (in this case the Spalart-Allmaras turbulent model) in the far field.

The IDDES implementation attempts to improve the transition between the LES and RANS regions. To do so, it uses a Wall Modeled LES technique, in which the inner-most part of the boundary layer is solved using RANS, while the turbulent phenomena that takes place inside the boundary layer is solved using LES. This way, even though the computational cost increases, the DDES approach is improved, by better developing the transition zone [21].

### 2.2.3. Mesh and Boundary Conditions

The computational domain is a cuboid of 36 m length, 12.6 m width and 7.75 m height ( $20 D \times 7 D \times 4.3 D$ ). The turbine is placed at the same 4.8 m from the inlet, however, it is positioned on the bottom face of the domain in such a way that there is no flow under the turbine. A series of mesh refinements were performed towards the turbine and in particular towards the blades. The idea was to refine the blades in order to better resolve the aerodynamic effects on these, therefore obtaining better results for the integral quantities as well as the wake and downwind velocities. The meshing for the blades was performed using the in-house tool “bladeBlockMesher” [22] while the rest of the turbine was meshed with the in-house “windTurbineMesher” tool [23]. Some of the details of the mesh generation can be observed in Figure 3. The resulting mesh consisted of approximately 32 million cells achieving a  $y^+$  value of 1.

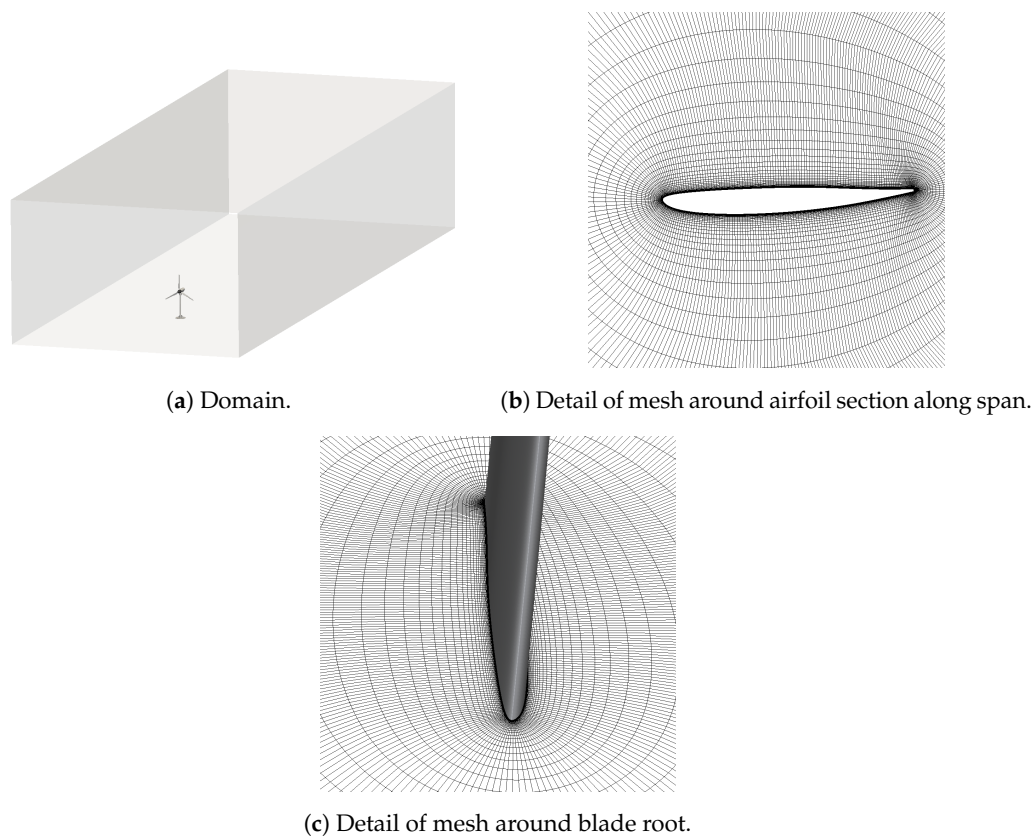


**Figure 3.** Computational mesh.

Except for the velocity and pressure, at the wall boundaries of the ‘Turbine’ group (blades, tower, hub, nacelle), wall functions were used, with the reference value indicated in Table 1. The ‘slip’ condition was set on the ‘Ground’ boundary, such that it better recreates the experiment’s conditions, according to Figure 2a. Since the turbine is not actually on the ground, a wall condition was not needed, instead the ‘slip’ condition was used. In order to use a dynamic mesh, to account for the rotor’s rotation (480 rpm), the rotating parts of the turbine (blades and hub) were set as moving walls. In particular, the blades were also set as cyclic Adaptive Mesh Interface (AMI) boundaries, taking into account that these would actually move through the domain, therefore modifying the mesh.

**Table 1.** Main boundary conditions.

Boundary	Velocity (m/s)	Pressure (Pa)	$k$ ( $\text{m}^2/\text{s}^2$ )	$\omega$ ( $\text{s}^{-1}$ )	$\nu_t$ ( $\text{m}^2/\text{s}$ )	$\nu_{sgs}$ ( $\text{m}^2/\text{s}$ )	$\nu'$ ( $\text{m}^2/\text{s}$ )
Inlet	6.03	zeroGradient	$6 \times 10^{-4}$	0.055	$4.5 \times 10^{-5}$	$3 \times 10^{-6}$	$3 \times 10^{-6}$
Outlet	zeroGradient	0	zeroGradient	zeroGradient	zeroGradient	zeroGradient	zeroGradient
Sky	slip	slip	slip	slip	slip	slip	slip
Ground	slip	slip	slip	slip	slip	slip	slip
Turbine	0	zeroGradient	$6 \times 10^{-4}$	0.055	$4.5 \times 10^{-5}$	$3 \times 10^{-6}$	$3 \times 10^{-6}$

### 3. Results

#### 3.1. Time Dependence

The first run of computations attempted to determine whether there was a dependency of the results with the resolution of the time-step. Three different time-steps were used:  $0.1^\circ$  per time step,  $0.5^\circ$  and  $1^\circ$  per time-step. For comparison, 10 seconds (80 rotations) of experimental data were considered. Figure 4 shows the results for the integral quantities (power, thrust, torque and blade-root bending moment ( $Mb_y$ ) in the flapwise direction) as a function of the azimuthal position of the rotor. As reference point, the azimuthal position of the blade was taken as  $0^\circ$  when the blade is at 12:00 (i.e., at its highest point).

There are several observations that can be made from Figure 4. First of all, it is clear that the model is able to recreate to a good extent the measurements. In particular, the tower shadow effect is clearly presented in each one of the graphs shown. This can be seen as the sudden decrease in the integral quantities, when one of the blades is aligned with the tower (i.e.,  $60^\circ$ ,  $180^\circ$  and  $300^\circ$  azimuth). In particular, Figure 4c shows that the experimental measurement for the torque is highly oscillating, due to the torque controller that the MoWiTO turbine uses. This is why in Figure 4a, the data for power is presented only at some specific azimuthal positions (every  $14.4^\circ$ ).

Regarding the thrust and the flapwise bending moment graphs, some inconsistent behavior could be observed. While the computational results for the thrust under-predict the experimental ones, the blade-root bending moment is over-predicted. The post-processing of the integral quantities was performed with an in-house tool. With this tool the thrust was calculated by integrating the aerodynamic force components of all the cells where the force was applied. Meanwhile, the bending moment is calculated discretely at 17 different sections along the span of the blade. Furthermore, we noticed that the velocity in the wake, at the root, was much smaller for the simulations than the experimental results (this will be presented afterwards in Figure 9). However, the opposite occurs for outer radial positions of the blade in the wake. This suggests that at the root of the blade, the thrust generated is larger for the simulations than for the experimental measurements. This could explain the differing behavior between the thrust and the blade-root bending moments, since the thrust calculated for Figure 4b is the complete thrust generated by the turbine, while the blade root bending moment in Figure 4d is accounted for only one blade, and is measured at the root. Therefore, knowing that the simulations are proving to show a larger thrust only at the root, the bending moment could be over-predicted while the thrust for the entire turbine is under-predicted. Nevertheless, the integral quantities prove to yield agreeable results overall. Table 2 shows the relative error between the

experimental results and the three different computational implementations. The error was calculated based on the average values of the results presented in Figure 4.

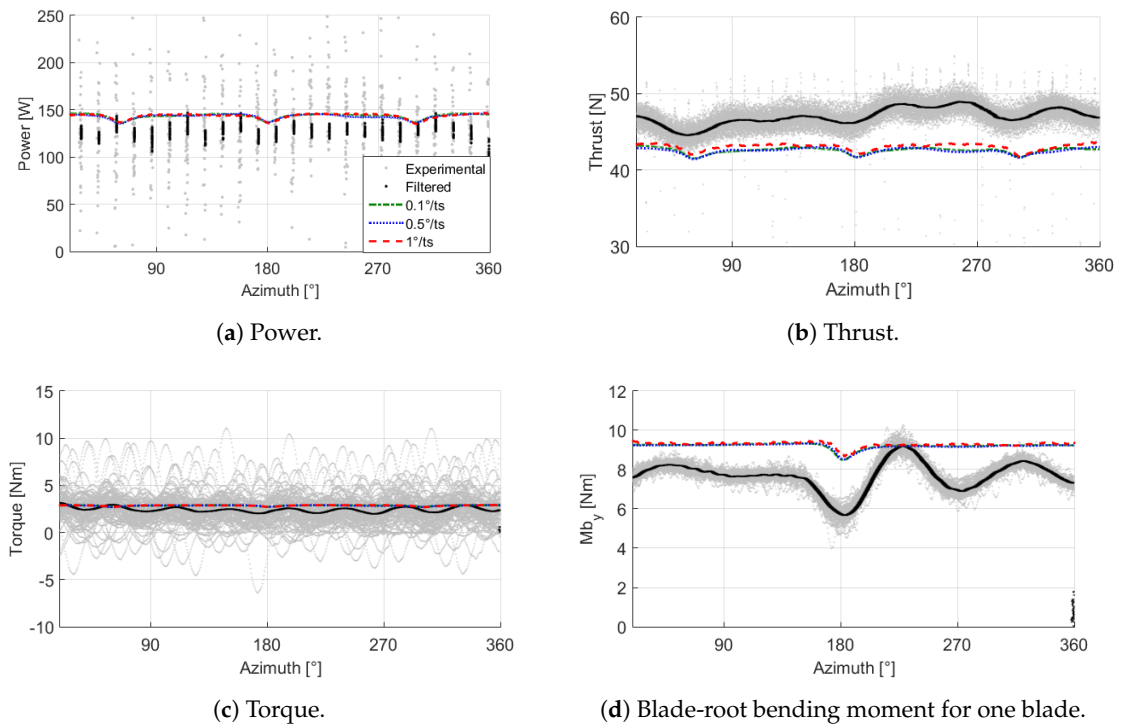


**Figure 4.** Comparison of azimuthal dependency of integral quantities, for time convergence.

**Table 2.** Comparison of the relative error for integral quantities, for time convergence analysis. Values are presented in percentage [%] unless indicated otherwise.

[°] per Time Step	Thrust	Torque	$Mb_y$	Avg. Error
0.1	9.42	12.76	20.04	14.07
0.5	9.58	12.31	19.85	13.91
1	8.40	12.69	21.13	14.07

In general, the relative errors are within the expected range. Power and torque have a higher relative error than expected, due to the large variations of the experimental torque. Regarding the blade root bending moment, the discrete post-processing technique might have some influence on the large relative error obtained. Additionally, it is evident that the experimental results are able to represent the elastic behavior of the turbine’s blade, since it shows an oscillation after the 180° mark. On the other hand, the simulations were performed assuming rigid bodies, which also influences the difference between the numerical and experimental results.

By averaging the relative errors of the integral quantities for each of the three different time steps used, it is evident that there is no major difference between the three time steps used. Even though the difference with respect to the other two time steps used is negligible (smaller than 0.1%), the results suggest that the 0.5° simulation is able to achieve the best results without incurring higher computational costs. This can be observed further in Figure 5.

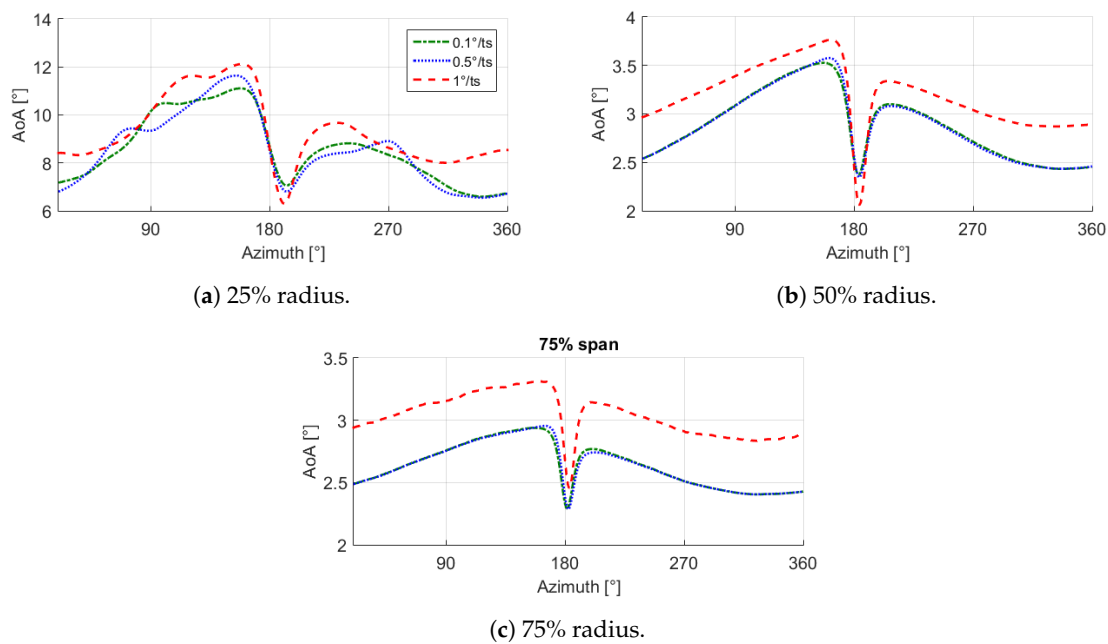


**Figure 5.** Angle of attack for one blade, at three different points along the blade span. The angle of attack was determined using Rahimi’s three point method [24,25].

In Figure 5 the evolution of the angle of attack along one rotation, can be seen as a function of the azimuthal position, using Rahimi’s 3-point method [24,25]. Unfortunately, due to the complexity of the flow characteristics, measuring with precision the experimental angle of attack at different azimuthal positions is highly complicated. However, the maximum angle of attack obtained of approximately  $12^\circ$ , does coincide with the static stall angle for the airfoil, obtained by Giguere and Selig [15]. Thus proving the accuracy and effectiveness of the 3-point method.

In addition, a correct behavior of the simulations can be seen, in particular by observing the tower shadow effect. That is, in this case, that the angle of attack reaches its lowest point after the blade passes the tower (i.e., after the  $180^\circ$  azimuthal position). Additionally, these graphs show that the  $0.5^\circ$  per time step implementation has a very similar behavior to the finest time resolution ( $0.1^\circ$ ), while the  $1^\circ$  per time-step implementation highly differs from the other two. Thus suggesting once again that the  $0.5^\circ$  per time step model, would yield good results at a reasonable computational cost.

### 3.2. DDES versus IDDES

#### 3.2.1. Integral Quantities

Once the time dependence analysis was concluded, a comparison between a DDES and an IDDES implementation was performed. In both cases the same boundary conditions and time-step were used ( $0.5^\circ$  of rotation per time-step). Once again, the integral quantities: power, thrust, torque and blade root bending moment were used as initial criteria for the comparison. These results can be observed in Figure 6.

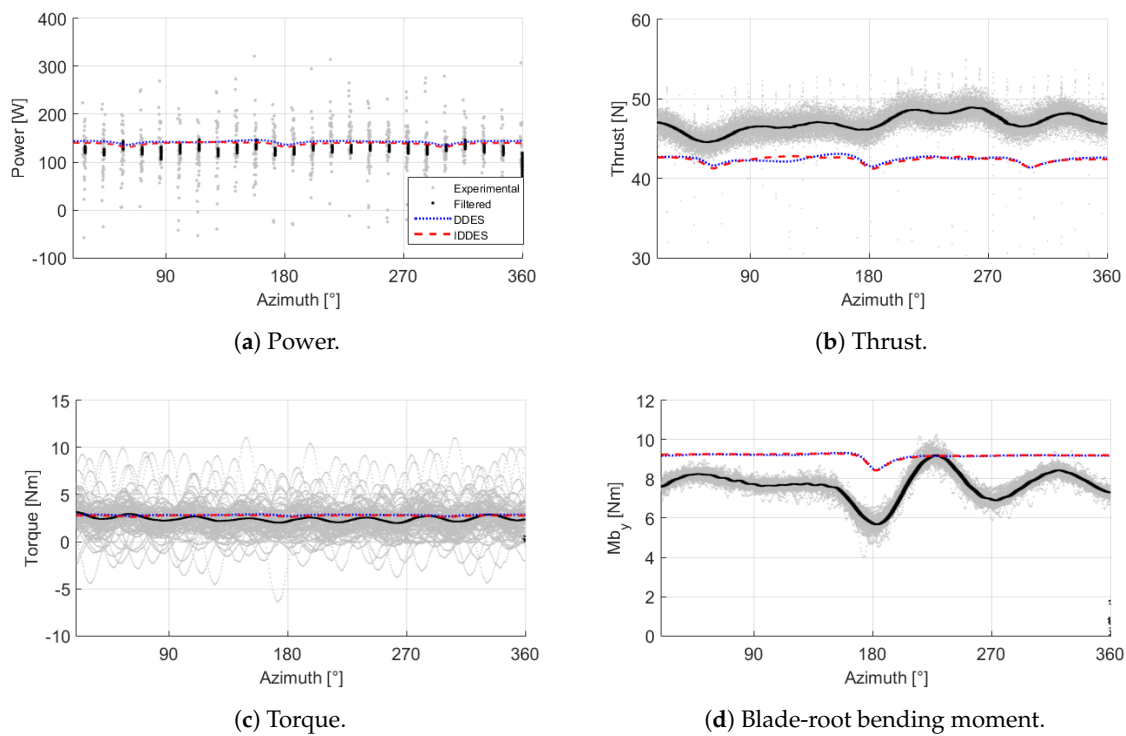


**Figure 6.** Comparison between Delayed Detached Eddy Simulation (DDES) and Improved DDES (IDDES) turbulent approach of the integral quantities.

Overall, both implementations show a very similar behavior. In both cases, the tower shadow effect is observed, as well as the inconsistency regarding the over/under-prediction of the thrust and the blade root bending moment. However, when looking at the relative errors (Table 3), it is evident that on average, the IDDES implementation is able to achieve better results. While the DDES implementation obtains an average error of 14.33%, the IDDES turbulent model is subject to a relative error of only 12.95%. Again, the difference is not truly outstanding, however, it is larger than the percentile differences according to Table 2.

**Table 3.** Relative error for integral quantities, for comparison between DDES and IDDES turbulent approach. Values are presented in percentage [%] unless indicated otherwise.

Turbulence Model	Thrust	Torque	$Mb_y$	Avg. Error
DDES	9.58	12.31	19.85	13.91
IDDES	9.97	8.87	19.67	12.84

It is expected that there are no major differences for the integral quantities' results, between the DDES and IDDES implementation. This is taking into account that both power and thrust are highly dependent on the behavior of the tip and root vortices, which are well captured by both turbulence models. The main difference between DDES and IDDES can be observed in the wake (as will be shown in Figures 7 and 11) rather than the boundary layer. According to Garbaruk et al. [26], whenever the simulation has an inlet with turbulent content, the majority of the turbulence is resolved, except in regions near the wall. Therefore, there should be no major differences between the tip and root vortices for both models, thus the difference in the integral quantities is also small.

Further information on the standard deviation of the data can be obtained by looking at the Power Spectral Density (PSD) graphs. In Figure 7 it can be observed the PSD for the thrust force, normalized per blade radius. For the section closest to the hub, both turbulent models behave in a very similar manner. Figure 7a in particular, shows that the energy content presents oscillations throughout the

entire frequency range. This suggests there is a high turbulent behavior, possibly due to the presence of the hub. This is confirmed in Figure 8 where the large vortical structures that are being formed towards the rotating axis of the turbine can be seen.

From Figure 8 it is also worth noting the presence of the tip vortices formed, as well as the tower shadow effect. The periodicity of the tip vortices is evident, where clear vortical structures can be observed towards the upper side of the turbine. Meanwhile, at the bottom, these same structures are disrupted by the vorticity that is shed from the tower. It is also interesting to notice the fact that the vortical structures that are formed behind the nacelle dissipate almost one turbine radius downstream. As a final remark on Figure 8, it can be observed that the vortices shed from the tower are of different sizes. Qualitatively, it is possible then, that the fluctuations that can be observed on the PSD's in Figure 7 are due to the interaction between these vortices and the blades.

For the other two radii it is evident that the energy content is focused on higher frequencies. However, when comparing Figure 7b,c for the DDES model a sudden spike close to the 160 Hz mark can be seen, but for the IDDES implementation this only occurs for the outboard section. In general, it can be seen that the IDDES turbulence model presents a higher energy content in comparison to the DDES. This is expected due to the improvement in the transition zone between the RANS and LES regions for DDES turbulence models. In this sense, by using an LES model to solve for the turbulent phenomena that take place inside the boundary layer, a better resolution of turbulent scales can be achieved such that the energy content for the IDDES simulation is higher (more eddies resolved, more turbulent energy). In addition, by being able to show further vortex shedding frequencies, the IDDES turbulence model proves to be useful when studying the performance of a turbine according to [3]. In particular, referring to the blade's structural integrity, therefore suggesting it could lead to better results when running an aeroelastic simulation. Unfortunately there was no experimental data available to compare with in order to justify the validity of either model, with the PSD as criteria.

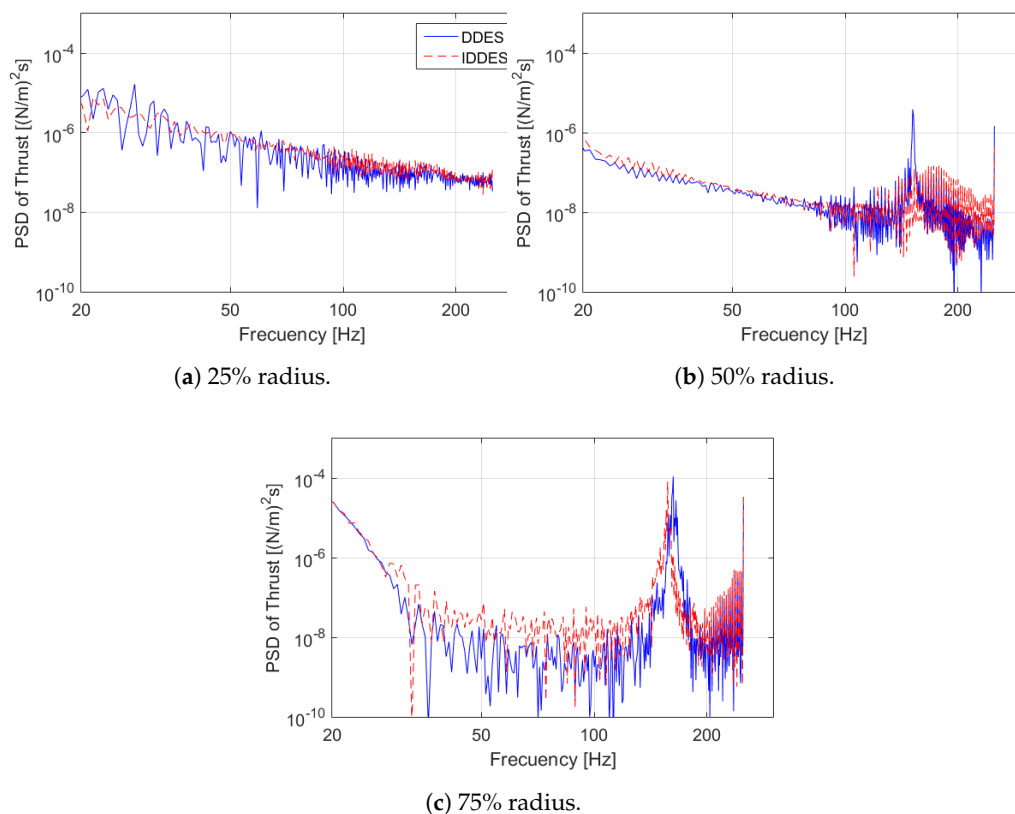


**Figure 7.** Power Spectral Density for the thrust normalized by blade radius, for 25%, 50% and 75% blade radius.

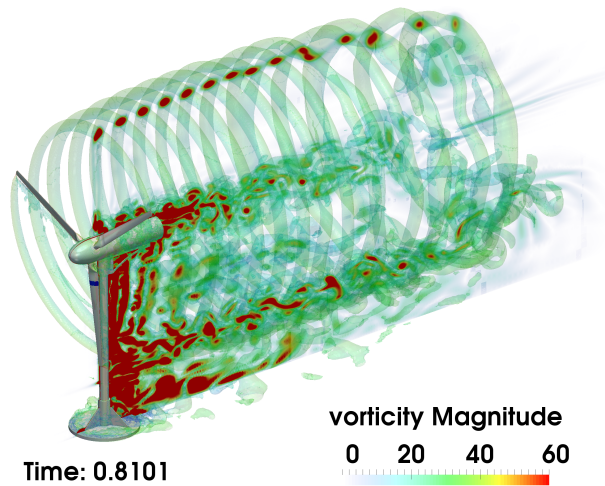


Figure 8. Vorticity visualization for the DDES turbulent simulation.

### 3.2.2. Velocity

A set of hot-wire measurements were taken at eight different points (from 0 to 1.4 radii, every 0.2 radii, from root to blade tip), 0.5 rotor diameters downwind of the rotor plane. This way, it was possible to do a comparison of the wake velocity in the longitudinal flow direction. The computational results presented in Figure 9 are the averages for only one rotation (0.125 s).

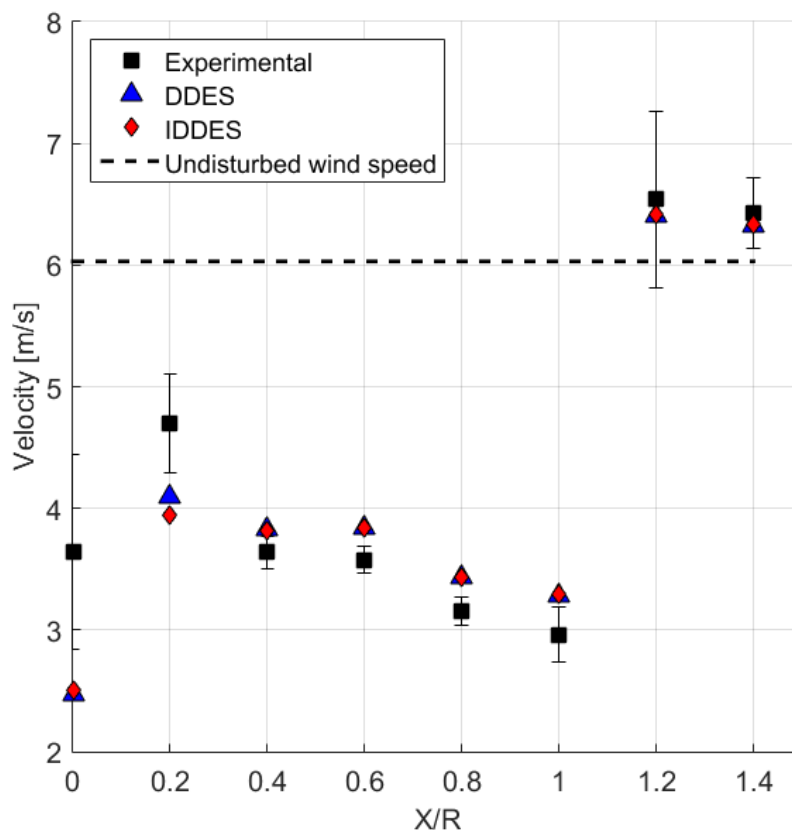


Figure 9. Average longitudinal velocity in the wake at 0.5D downstream. Average for one rotation.

Once again, a good agreement between the numerical and experimental results is achieved. With the exception of the measurements at 0 and 0.2 radii, both turbulent implementations present a very similar behavior. This is expected, taking into account that for the two probes closest to the hub and nacelle there are high turbulent fluctuations present. This has been shown in experiments such as

the ones performed by Akay et al. [27] where the intricacies of root flow are confirmed. In order to evaluate quantitatively how the computational results differ from the experimental ones, Figure 9 and Table 4 show the average velocity for each probe in the wake.

**Table 4.** Relative error for wake measurements 0.5 diameters behind the rotor plane, at eight different positions from 0 to 1.4 radii from root to blade tip.

Radial Position (X/R)	Error (%)	
	DDES	IDDES
0	36.17	29.44
0.2	17.15	20.03
0.4	2.37	2.27
0.6	5.14	5.16
0.8	7.77	7.75
1.0	7.76	7.77
1.2	3.86	3.77
1.4	5.42	5.35

Overall a good agreement can be observed between both computational models and the experimental measurements. With the exception of the first two probes (0 and 0.2 radii), the relative errors are lower than 8%. Once again, the IDDES implementation is able to obtain a smaller relative error on average. While the DDES implementation attains a 10.71% average relative error, the IDDES model obtains a 10.19% relative error average. In this case, the difference is not as notorious as for the integral quantities, however, this supports once again the fact that the IDDES implementation is able to obtain the most agreeable results. Even more, it is able to do so in a very similar computational time as the DDES implementation.

### 3.2.3. Forces

It was decided also to look at the behavior of the tangential and normal forces at different sections along the blade radius. This was intended to compare the aerodynamic behavior of both implementations. In Figure 10 the results for the normal ( $C_n$ ) and tangential ( $C_t$ ) force coefficients can be observed, at three different sections along the blade radius.

It is clear that there is great agreement between the turbulence models for the normal and tangential forces on the outbound sections of the blade, as can be seen in Figure 10. However, for the inbound section at 25% of blade radius there is great disparity. Even though the values obtained for both  $C_n$  and  $C_t$  are within the same orders of magnitude (thus proving the correct implementation of both models), they do display very different behaviors. This is taking into account that there are more vortical structures towards the center of the rotor due to the presence of the hub and nacelle, as it is observed in Figures 7 and 8.

In a similar way, Figure 11 demonstrates there is no great discrepancy in the wall shear stress for the DDES and IDDES turbulent model. This figure shows the wall shear stress at the suction side, for two different azimuthal angles, for both DDES and IDDES turbulent models. These images validate that the flow is only separated at the root, and barely at the tip of the blade. The main difference in this case, is that the flow separation for the DDES model happens approximately at the 40% span, while for the IDDES model it occurs closer to the 30% section. Looking towards the tip of the blade, at the trailing edge, it is clear that there is some separation which leads to the formation of the tip vortices. In this case, it can be seen that for the IDDES model, this separation is more evident. This is where the major advantage of using IDDES can be observed. Should the turbine be set at a more critical condition (i.e., larger pitch angles), the effect of separation should be even more noticeable. This is taking into account that the separation phenomenon in the IDDES simulation is occurring closer to the root, and more defined towards the tip. Thus suggesting that this separation is a better

representation of the physical phenomenon, instead of the DDES which has some numerical effects that lead to separation further along the blade's span.

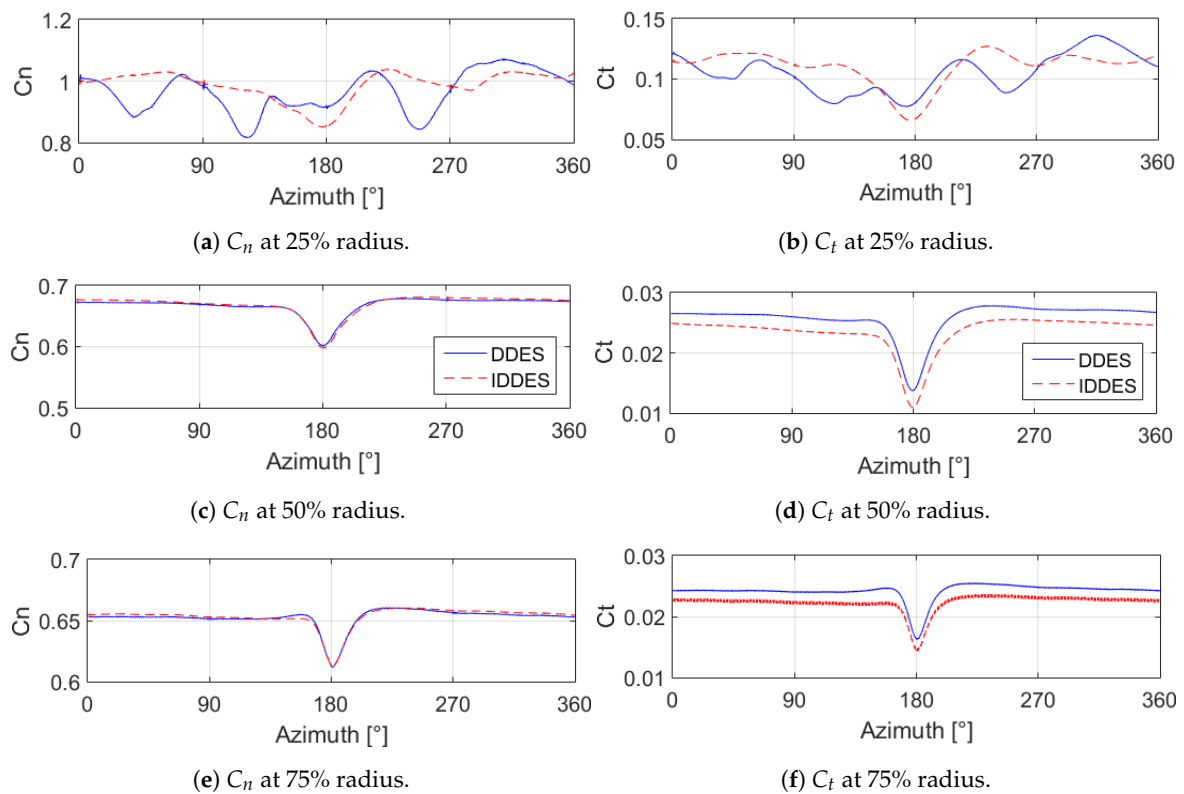


Figure 10. Normal and tangential force coefficients for three different sections along a blade radius.

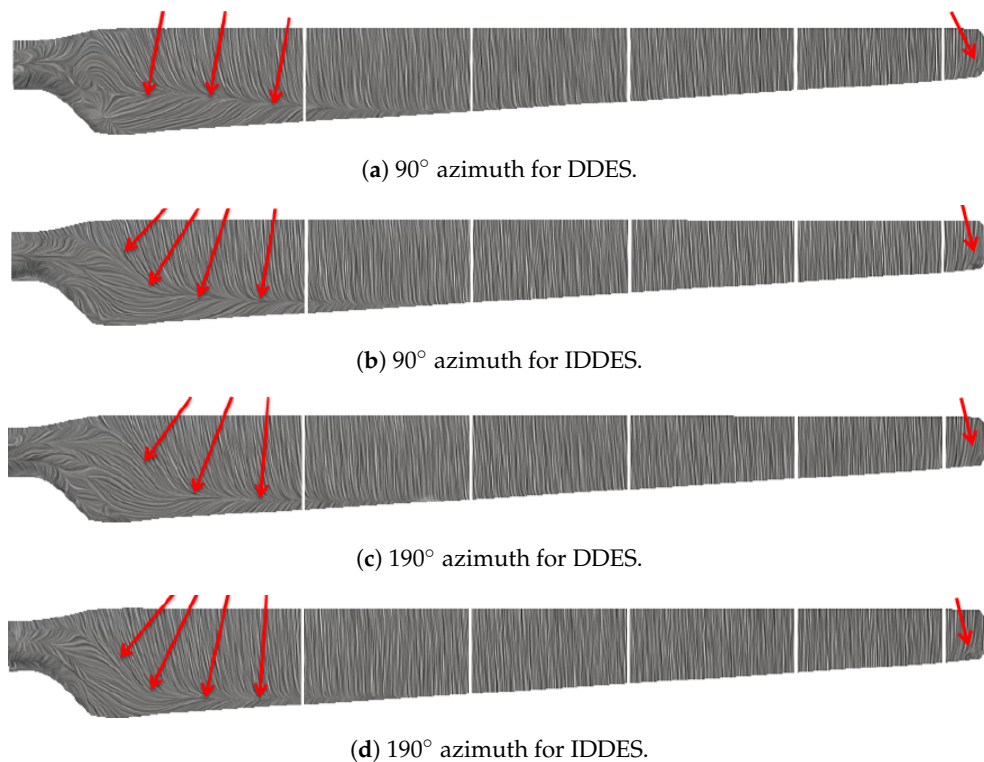


Figure 11. Comparison of wall shear stress between Improved DDES and DDES for one blade, at two different azimuthal positions. The five vertical lines indicate the location of the 30%, 47%, 63%, 80% and 95% sections.

### 3.2.4. Computational Cost

All simulations were run in the HPC EDDY of ForWind—University of Oldenburg. The DDES and IDDES implementations were parallelized using 408 processors. While the DDES simulation took approximately 101 h to complete 2.5 s of simulation (20 turbine rotations), the IDDES implementation took 104 h. Therefore, it can be stated that an IDDES implementation with  $0.5^\circ$  of rotation per time step, yields agreeable results without incurring higher computational costs, for the MoWiTO 1.8 model turbine.

## 4. Conclusions

A series of numerical simulations were performed in order to simulate the Model Wind Turbine Oldenburg (MoWiTO 1.8). Two sets of simulations were performed; the first to evaluate the time dependence of the results and the second one to compare the results obtained by two different turbulent implementations.

Overall it could be observed that all simulations were able to obtain agreeable results between the numerical and the experimental results. In particular, from the time dependence analysis, it could be observed that the integral quantities (power, thrust, torque and blade root bending moment) had acceptable relative errors. In particular, the implementation using  $0.5^\circ$  of azimuthal rotation per time step, proved to achieve the best results.

In general, all simulations proved to model the phenomena correctly. All simulations were able to reproduce the tower shadow effect, demonstrating that the dynamic mesh model was correctly implemented. On the other hand, the PSD graphs and the vorticity visualization help to validate the correct use of the boundary conditions, in particular by being able to recreate the vortical structures near the rotor's axis and the tip vortices. It could also be stated that an IDDES turbulent implementation using  $0.5^\circ$  of rotation per time step, with a mesh of 32 million cells, is able to achieve good results without incurring higher computational costs. Furthermore, the evolution of the angle of attack as a function of the azimuthal position (Figure 5), validates once again the accuracy of the 3-point method developed by Rahimi et al. [24].

Regarding the comparison of turbulent models, the results for integral quantities do not show great differences. The DDES implementation has an average relative error of 13.91%, while the IDDES is able to decrease this reaching a value of 12.84%. Looking at the wake measurements, 0.5 diameters downwind from the rotor plane, it could be observed once again that IDDES implementation is able to achieve results closer to the experimental data than the DDES turbulent model. Additionally, it is worth mentioning that the IDDES is able to obtain these results in slightly less computational time. However, the PSD and velocity results did show that IDDES is able to resolve better the vortex shedding frequencies. Therefore, it could be suggested that an IDDES turbulence model is a better option than DDES, when studying the wake's behavior. In a similar way, by resolving these frequencies, it could also give a better insight into the blades' structural stability, thus in aeroelastic analyses.

Further validations can and should be performed for this turbine. In particular, it would be interesting to perform an aeroelastic simulation in order to consider the elastic effects of the turbine blades. In addition, by running another set of experiments on the wind tunnel, a good insight on the behavior of the turbine could be achieved, under different inflow conditions. Simulations on these conditions could be validated by such results, further proving the effectiveness of these computational tools. In a similar way, by setting the turbine at different yaw angles, and different pitch angles for the blades, a more critical condition could be evaluated. It would be expected, that in these new conditions, greater differences could be observed between the two turbulent models (i.e., in the wake or the wall shear stress).

**Author Contributions:** Conceptualization, C.S., F.B. and H.R.; Methodology, C.S., F.B. and H.R.; Software, C.S. and H.R.; Formal Analysis, C.S.; Writing—Original Draft Preparation, C.S. except section 2.1 which was written by F.B.; Writing—Review & Editing, H.R., O.L. and M.K.; Supervision & Project Administration, M.K. and B.S.

**Funding:** F.B. acknowledges funding for the experiments by the Ministry for Science and Culture of Lower Saxony through the funding initiative Niedersächsisches Vorab (project ventus efficiens).

**Acknowledgments:** The authors would like to thank the HPC support team at the University of Oldenburg, for providing the cluster computing service in which the simulations were performed.

**Conflicts of Interest:** The authors declare no conflict of interest.

## References

1. Haans, W. Wind Turbine Aerodynamics in Yaw: Unravelling the Measured Rotor Wake. Ph.D. Thesis, Delft University of Technology, Delft, The Netherlands, 2011.
2. European Energy Research Alliance. AVATAR: Advanced Aerodynamic Tools for Large Rotors. 2016. Available online: <http://www.eera-avator.eu/> (accessed on 9 September 2018).
3. Rahimi, H.; Dose, B.; Stoevesandt, B.; Peinke, J. Investigation of the validity of BEM for simulation of wind turbines in complex load cases and comparison with experiment and CFD. *J. Phys. Conf. Ser.* **2016**, *749*, 1–9. [[CrossRef](#)]
4. Rahimi, H.; Martinez, A.; Stoevesandt, B.; Peinke, J.; Schepers, G. An engineering model for wind turbines under yawed conditions derived from high fidelity models. *Wind Energy* **2018**, *21*, 618–633. [[CrossRef](#)]
5. Hand, M.; Simms, D.; Fingersh, L.; Jager, D.; Cotrell, J.; Schreck, S.; Larwood, S. *Unsteady Aerodynamics Experiment Phase VI: Wind Tunnel Test Configurations and Available Data Campaigns*; National Renewable Energy Laboratory: Golden, CO, USA, 2001; NREL/TP-500-29955.
6. Sorensen, N.N.; Michelsen, J.A.; Schreck, S. Navier-Stokes Predictions of the NREL Phase VI Rotor in the NASA Ames 80 ft × 120 ft Wind Tunnel. *Wind Energy* **2002**, *5*, 151–169. [[CrossRef](#)]
7. Sorensen, N.N.; Schreck, S. Transitional DDES computations of the NREL Phase-VI rotor in axial flow conditions. *J. Phys. Conf. Ser.* **2014**, *555*, 1–10. [[CrossRef](#)]
8. Zahle, F.; Sorensen, N.N.; Johansen, J. Wind Turbine Rotor-Tower Interaction Using an Incompressible Overset Grid Method. *Wind Energy* **2009**, *12*, 594–619. [[CrossRef](#)]
9. Rahimi, H.; Medjroubi, W.; Stoevesandt, B.; Peinke, J. Navier-Stokes-based predictions of the aerodynamic behavior of stall regulated wind turbines using OpenFOAM. *Prog. Comput. Fluid Dyn.* **2016**, *16*, 339–355. [[CrossRef](#)]
10. Länger-Möller, A.; Löwe, J.; Kessler, R. Investigation of the NREL phase VI experiment with the incompressible CFD solver THETA. *Wind Energy* **2017**, *20*, 1529–1549. [[CrossRef](#)]
11. Gritskevich, M.S.; Garbaruk, A.V.; Schütze, J.; Menter, F.R. Development of DDES and IDDES Formulations for the  $k-\omega$  Shear Stress Transport Model. *Flow Turbul. Combust.* **2012**, *88*, 431–449. [[CrossRef](#)]
12. Rahimi, H.; Dose, B.; Herráez, I.; Peinke, J. DDES and URANS comparison of the NREL VI wind turbine at deep stall. In Proceedings of the 34th AIAA Applied Aerodynamics Conference, Washington, DC, USA, 13–17 June 2016; pp. 1–16. [[CrossRef](#)]
13. Berger, F.; Kühn, M. Experimental investigation of dynamic inflow effects with a scaled wind turbine in a controlled wind tunnel environment. *J. Phys. Conf. Ser.* **2018**, *1037*, 1–10. [[CrossRef](#)]
14. Jonkman, J.; Butterfield, S.; Musial, W.; Scott, G. *Definition of a 5-MW Reference Wind Turbine for Offshore System Development*; National Renewable Energy Laboratory: Golden, CO, USA, 2009; NREL/TP-500-38060.
15. Giguere, P.; Selig, M.S. New Airfoils for Small Horizontal Axis Wind Turbines. *ASME J. Sol. Energy Eng.* **1998**, *120*, 108–114. [[CrossRef](#)]
16. OpenCFD. OpenFOAM—The Open Source CFD Toolbox—User’s Guide. 2018. Available online: <http://openfoam.org> (accessed on 23 January 2019).
17. Versteeg, H.K.; Malalasekera, W. *An Introduction to Computational Fluid Dynamics—The Finite Volume Method*; Pearson Prentice Hall: Glasgow, UK, 2007; ISBN 978-0-13-127498-3.
18. The University of Oldenburg. The HPC User Wiki of the University of Oldenburg. Carl von Ossietzky Universität Oldenburg. Available online: <https://uol.de/en/school5/sc/high-performance-computing/introduction-hpc/> (accessed on 23 January 2019).
19. Spalart, P.R. Strategies for turbulence modelling and simulations. *Int. J. Heat Fluid Flow* **2000**, *21*, 252–263. [[CrossRef](#)]
20. Spalart, P.R.; Deck, S.; Shur, M.; Squires, K.; Strelets, M.K.; Travin, A. A new version of detached-eddy simulation, resistant to ambiguous grid densities. *Theor. Comput. Fluid Dyn.* **2006**, *20*, 181–195. [[CrossRef](#)]

21. Shur, M.L.; Spalart, P.R.; Strelets, M.K.; Travin, A.K. A hybrid RANS-LES approach with delayed-DES and wall-modeled LES capabilities. *Int. J. Heat Fluid Flow* **2008**, *29*, 1638–1649. [[CrossRef](#)]
22. Rahimi, H.; Daniele, E.; Stoevesandt, B.; Peinke, P. Development and application of a grid generation tool for aerodynamic simulations of wind turbines. *Wind Eng.* **2016**, *40*, 148–172. [[CrossRef](#)]
23. Rahimi, H. Validation and Improvement of Numerical Methods for Wind Turbine Aerodynamics: Development of an Engineering Model for Yawed Conditions Derived From Computational Fluid Dynamics. Ph.D. Thesis, University of Oldenburg, Oldenburg, Germany, 2018.
24. Rahimi, H.; Hartvelt, M.; Peinke, J.; Schepers, J.G. Investigation of the current yaw engineering models for simulation of wind turbines in BEM and comparison with CFD and experiment. *J. Phys. Conf. Ser.* **2016**, *753*, 1–14. [[CrossRef](#)]
25. Vimalakanthan, K.; Schepers, J.G.; Shen, W.Z.; Rahimi, H.; Micallef, D.; Simao Ferreira, C.J.; Jost, E.; Klein, L. Evaluation of different methods of determining the angle of attack on wind turbine blades under yawed inflow conditions. *J. Phys. Conf. Ser.* **2018**, *1037*, 1–11. [[CrossRef](#)]
26. Garbaruk, A.; Shur, M.; Strelets, M.; Sparlat, P.R.; Balakrishnan, R. DDES and IDDES of Tandem Cylinders. In Proceedings of the Benchmark Problems for Airframe Noise Computations BANC, Orlando, FL, USA, 4–7 January 2011; pp. 1–12.
27. Akay, B.; Micallef, D.; Simao Ferreira, C.J.; van Bussel, G.J.W. Effects of geometry and tip speed ratio on the HAWT blade's root flow. *J. Phys. Conf. Ser.* **2014**, *555*, 1–15. [[CrossRef](#)]



© 2019 by the authors. Licensee MDPI, Basel, Switzerland. This article is an open access article distributed under the terms and conditions of the Creative Commons Attribution (CC BY) license (<http://creativecommons.org/licenses/by/4.0/>).